2017/09/04
Head Id: 423401
Archive Id: 423465:423468
Archive Date: 2017/09/01
Archive Tag: trunk

Measurement of the production cross section of a single top quark and a W boson in pp collisions at $\sqrt{s}$ = 13 TeV

The CMS Collaboration

Abstract

A measurement of the associated production of a single top quark and a W boson in pp collisions at $\sqrt{s} = 13$ TeV with the CMS experiment at the CERN LHC is presented. The analyzed data, collected in 2016, corresponds to an integrated luminosity of 35.9 fb^{-1}. The measurement is performed in the dilepton final state, using events with one electron and one muon. A multivariate discriminant, exploiting kinematic properties of events, is used to separate the signal from the dominant $\mathrm{t\bar{t}}$ background. A cross section of $\sigma = 63.1 \pm 1.8\ (\text{stat}) \pm 5.7\ (\text{syst}) \pm 2.1\ (\text{lumi})$ pb is measured, in agreement with the standard model expectation.

1 Introduction

Single top quarks, observed for the first time by the CDF [1] and D0 [2] experiments at the Tevatron, are produced via the electroweak interaction. There are three different production modes: the exchange of a virtual W boson (t-channel), the production and decay of a virtual W boson (s-channel), and the associated production of a top quark in association with a W boson (tW channel). The study of tW production at the LHC at CERN provides unique opportunities for studying the standard model (SM) and its extensions: its production interferes at next-to-leading order (NLO) with top quark pair production [3–5]; it is sensitive to new physics [6–8]; and has an important role as a background to SUSY and Higgs searches.

The tW production channel, negligible at the Tevatron because of its small production rate in $p\bar{p}$ collisions at $\sqrt{s}$ = 1.96 TeV, represents a significant contribution to single top quark production at the LHC. The CMS and ATLAS Collaborations presented evidences [9, 10] and observations [11, 12] of this process with 7 and 8 TeV collision data, respectively, and the measured cross sections are in good agreement with the prediction from the SM. The ATLAS Collaboration measured the production cross section using 13 TeV data [13].

The tW production cross section has been computed at approximate next-to-next-to-leading-order (aNNLO), the theoretical prediction of the tW cross section in pp collisions at $\sqrt{s}$ = 13 TeV, assuming a top-quark mass (m_t) of 172.5 GeV, is 71.7 ± 1.8 (scale) ± 3.4 (PDF) pb [14]. The leading order Feynman diagrams for tW production are shown in Fig. 1.

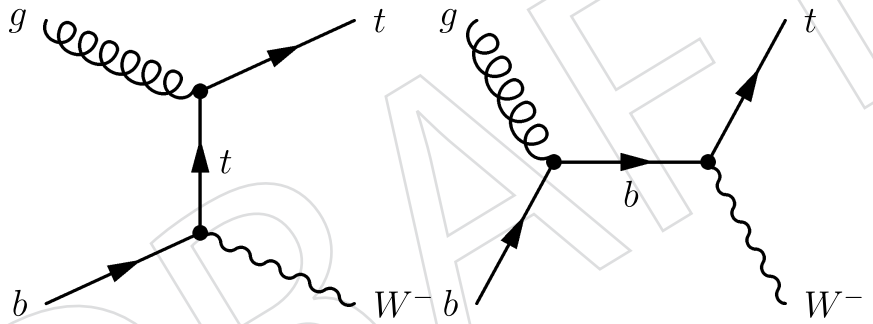

Figure 1: Leading order Feynman diagrams for single top quark production in the tW mode, the charge-conjugate modes are implicitly included.

This paper reports the first measurement from the CMS experiment of tW production in pp collisions at $\sqrt{s}$ = 13 TeV. The measurement uses the full data set recorded by CMS at 13 TeV during 2016, which corresponds to an integrated luminosity of $\mathcal{L} = 35.9 \pm 0.9$ fb^{-1}. The analysis is performed using the dilepton ($e^{\pm}\mu^{\mp}$) decay channel, in which the W boson produced in association with the top quark and the W boson from the decay of the top quark both decay leptonically into a muon or an electron, and a neutrino. The primary background to tW production in this final state comes from top quark pair production ($t\bar{t}$) production, with Drell-Yan (DY) events being the next most significant. To extract the signal, the analysis uses a multivariate technique, exploiting kinematic and topological differences to distinguish the tW signal from the dominant $t\bar{t}$ background.

The paper is structured as follows. Section 2 gives a summary of the CMS detector and of the Monte Carlo (MC) simulation samples used. The object and event selections are discussed in Section 3. The description of the method used to separate the tW signal from the $t\bar{t}$ background is shown in Section 4. The different sources of systematic uncertainties are discussed in Section 5. The tW production cross section extraction is described in Section 6 and a summary of

the results obtained is presented in Section 7.

2 The CMS detector and Monte Carlo simulation

The CMS detector [15] has a superconducting solenoid in its central region that provides an axial magnetic field of 3.8 T. The silicon pixel and strip trackers cover $0 < \phi < 2\pi$ in azimuth and $|\eta| < 2.5$ in pseudorapidity. The lead tungstate crystal electromagnetic calorimeter, and the brass and scintillator hadron calorimeter are located inside the solenoid. These are used to identify electrons, photons and jets. Muons are measured in gas-ionization detectors embedded in the steel flux-return yoke outside the solenoid. The detector is nearly hermetic, providing reliable measurement of the momentum imbalance in the plane transverse to the beams. A two-level trigger system selects the most interesting pp collisions for offline analysis. A more detailed description of the CMS detector, together with a definition of the coordinate system used and the relevant kinematic variables, can be found in Ref. [15].

The single top tW signal process is simulated at NLO using POWHEG v1 [16] with the NNPDF 3.0 PDF set [17], and PYTHIA v8.2 [18, 19] with the CUETP8M1 [20, 21] tune is used for parton showering. At NLO, the definition of tW production in perturbative QCD interferes with $\mathrm{t\bar{t}}$ production [3–5]. Two different procedures are used to deal with this interference: "diagram removal" (DR) [3], where all NLO diagrams which are doubly resonant are excluded from the signal definition; and "diagram subtraction" (DS) [3, 22], in which the differential cross section is modified with a gauge-invariant subtraction term, that locally cancels the contribution of $\mathrm{t\bar{t}}$ diagrams. The DR scheme is used here, but it has been verified that the number of predicted events after full selection is comparable with the DS approach.

The NLO POWHEG v2 [23] setup, with turning the damping parameter (h_{damp}) on, is used to simulate $\mathrm{t\bar{t}}$ events and the dependency of the $\mathrm{t\bar{t}}$ modelling on m_t, the renormalization and factorization scale (Q^2), and the PDFs. The NNPDF 3.0 set is used as default PDF. The $\mathrm{t\bar{t}}$ events are showered using PYTHIA v8.2 with the CUETP8M2T4 tune [24].

Besides the $\mathrm{t\bar{t}}$ background process, the other background contributions are also estimated from MC simulations. The DY and W+jets background samples are generated with MG5_aMC@NLO v5_2.2.2 [25] with NNPDF 3.0 and interfaced to PYTHIA v8.2 with the CUETP8M1 tune for hadronization and fragmentation. Z-bosons are simulated with up to two additional partons and the FxFx scheme [26] is used for the merging. The generation is split into two distinct $\ell^+\ell^-$ invariant mass ranges: $10 < M_{\ell^+\ell^-} < 50$ GeV and $M_{\ell^+\ell^-} > 50$ GeV. The contributions from WW, WZ, and ZZ (referred to as "VV") processes are simulated with PYTHIA v8.2 with the CUETP8M1 tune. Other contributions from W and Z boson production in association with $\mathrm{t\bar{t}}$ events (referred to as "$\mathrm{t\bar{t}V}$") are simulated using MG5_aMC@NLO v5_2.2.2 and PYTHIA v8.2. Finally, $\mathrm{t\bar{t}}$ or W+jets events in the lepton+jets final state with a jet incorrectly reconstructed as a lepton or with a lepton incorrectly identified as being isolated are also taken into account. These events, included in the samples described above, are classified into the nonprompt leptons category ("non-W/Z") since prompt leptons are defined as originating from decays of W or Z boson.

For comparison with the measured distributions, the event yields in the simulated samples are normalized to the corresponding integrated luminosity and their theoretical cross sections. These are taken from NNLO (W+jets and DY [27]), aNNLO (single top quark tW-channel [14]), and NLO (diboson [28]) calculations. For the simulated $\mathrm{t\bar{t}}$ sample, the full NNLO+NNLL calculation, performed with the TOP++ 2.0 program [29], is used. The PDF and α_S uncertainties are estimated using the PDF4LHC prescription [30, 31] with the MSTW2008, CT10 NNLO [32, 33],

and NNPDF2.3 5f FFN [34] PDF sets, and added in quadrature to the scale uncertainty to obtain a $\mathrm{t\bar{t}}$ production cross section of $832\,^{+20}_{-29}\,(\mathrm{scale}) \pm 35(\mathrm{PDF}+\alpha_s)$ pb assuming m_t=172.5 GeV. The simulated samples include additional interactions per bunch crossing (pileup), with the distribution matching that observed in data, with an average of about 27 collisions per bunch crossing.

3 Event selection

In the SM, top quarks decay almost exclusively into a W boson and a b quark. The analysis is performed using the $\mathrm{e}^{\pm}\mu^{\mp}$ decay channel, in which the W boson produced in association with the top quark and the W boson from the decay of the top quark both decay leptonically, one into an electron and the corresponding neutrino, the other into a muon and the corresponding neutrino. This leads to a final state composed of two oppositely charged isolated leptons, a jet resulting from the fragmentation of a b quark, and two neutrinos. The event selection described here follows closely the one used in the measurement of the top quark-antiquark pair production cross section in the dilepton channel [35].

Events are required to pass either a dilepton or single lepton trigger. The dilepton triggers require events to contain either one electron with transverse momentum $p_{\mathrm{T}} > 12$ GeV and one muon with $p_{\mathrm{T}} > 23$ GeV or one electron with $p_{\mathrm{T}} > 23$ GeV and one muon with $p_{\mathrm{T}} > 8$ GeV. In addition, single-lepton triggers with one electron (muon) with $p_{\mathrm{T}} > 27$ GeV (24) are used in order to increase the efficiency. The efficiency for the combination of the single lepton and dilepton triggers is measured in data using triggers based on p_{T} imbalance in the event. The trigger in simulation is corrected using a multiplicative data-to-simulation scale factor (SF), given by the trigger efficiency measured in data with independent monitoring triggers.

The particle-flow (PF) event algorithm [36] reconstructs and identifies each individual particle with an optimized combination of information from the various elements of the CMS detector. Selected dilepton events are required to contain one isolated electron [37] and one isolated muon [38] with opposite electric charges and $p_{\mathrm{T}} > 20$ GeV and $|\eta| < 2.4$. Isolation requirements are based on the ratio of the scalar sum of the transverse momenta of all PF candidates, reconstructed inside a cone centered on the lepton, excluding the contribution from the lepton candidate. This isolation variable is required to be smaller than 6% (15%) of the electron (muon) p_{T}. Events with W bosons decaying into τ leptons contribute to the measurement only if the τ leptons decay into electrons or muons that satisfy the selection requirements. In events with more than two leptons passing the selection, the two with the largest p_{T} are selected for further study.

Jets are reconstructed from the PF candidates using the anti-k_{T} clustering algorithm [39, 40] with a distance parameter of 0.4. The jet momentum is determined from the vectorial sum of all particle momenta in the jet, and is estimated, from simulation, to be within 5 to 10% of the true momentum over the whole p_{T} spectrum and detector acceptance. An offset correction is applied to jet energies to take into account the contribution from additional proton-proton interactions within the same or nearby bunch crossings. Jet energy corrections are derived from simulation, confirmed with in situ measurements of the energy balance in dijet and photon + jet events, and are applied as a function of the jet p_{T} and η [41] to both data and simulated events. Jets are required to have $p_{\mathrm{T}} > 30$ GeV and $|\eta| < 2.4$. In order to avoid double counting, jets within a ΔR cone of 0.4 with respect to the selected leptons are not considered. Jets passing looser kinematic selection (referred to as "loose jets") are required to have p_{T} between 20 and 30 GeV and $|\eta| < 2.4$.

The missing transverse momentum vector, $\vec{p}_{\mathrm{T}}^{\,\mathrm{miss}}$, is defined as the negative vector sum of the momenta of all reconstructed PF candidates in an event, projected onto the plane perpendicular to the direction of the proton beams. Its magnitude is referred to as $p_T^{miss}$and the corrections to jet momenta are propagated to the p_T^{miss}calculation [42].

Unlike some of the backgrounds, such as DY events, the tW final state contains a b quark. The identification of jets originating from b quarks reduces significantly the background contamination. Jets are identified as b jets using the combined secondary vertex algorithm v2 [43, 44], with an operating point which yields identification efficiencies of $\simeq 70\%$ and a misidentification (mistag) probabilities of about 1% and 15% [44] for light-flavor jets (u, d, s, and gluons) and c jets, respectively, estimated in simulated events.

Events are classified as belonging to the $\mathrm{e}^{\pm}\mu^{\mp}$ final state if the two leading leptons passing the above selection criteria are an electron and a muon of opposite charge. We require the leading lepton to have $p_{\mathrm{T}} > 25$ GeV. To reduce the contamination from DY background, the invariant mass of the lepton pair is required to be greater than 20 GeV. Figure 2 shows data and simulation for several lepton kinematic variables after this baseline selection. In general, good agreement is observed.

Figure 3 shows a comparison of the yields observed in data with the ones estimated from simulated events, classified according to the number of jets and identified b jets in the event. As expected, most of the signal events populate the region with one jet which is tagged as a b jet (1j1b region), but the amount of signal in comparison with the overwhelming $\mathrm{t\bar{t}}$ background makes a cut based analysis extremely challenging. Therefore, a multivariate analysis is pursued.

For the final analysis, events in the 1j1b signal region are used, as well as two background dominated control regions. The background control regions are defined as events with exactly two jets which have exactly one b-tagged jet (2j1b region) and which have both jets b-tagged (2j2b region).

4 Signal extraction

As referred to previously, after the baseline event selection is performed, the data sample in the 1j1b region consists primarily of $\mathrm{t\bar{t}}$ events with a significant number of tW signal events (see Fig. 3). Given there is no single observable that clearly discriminates between the signal and background, a multivariate method is used in order to provide discrimination between the tW signal and $\mathrm{t\bar{t}}$ events, the main background process. Several observables are combined into a single discriminator using a boosted decision tree (BDT) technique [45]. In this analysis, the BDT implementation is provided by the "Toolkit for Multivariate Data Analysis" (TMVA) [46] package, using the GradientBoost algorithm. The training of the BDT is performed using dedicated samples for tW and $\mathrm{t\bar{t}}$, statistically independent from the ones used for the signal extraction. The input variables used for the training of the BDT in the 1j1b region, listed in order of importance to the BDT training, are the following:

- p_{T} of leading loose jet, defined as 0 for events with no loose jets present,
- vector sum of the p_{T} of leptons, jet, and $\vec{p}_{\mathrm{T}}^{\,\mathrm{miss}}$ (p_T^{sys}),
- p_{T} of the leading, tight, b-tagged jet,
- ratio of scalar sum of p_{T} of the leptons to the H_T of full system,
- number of loose jets,

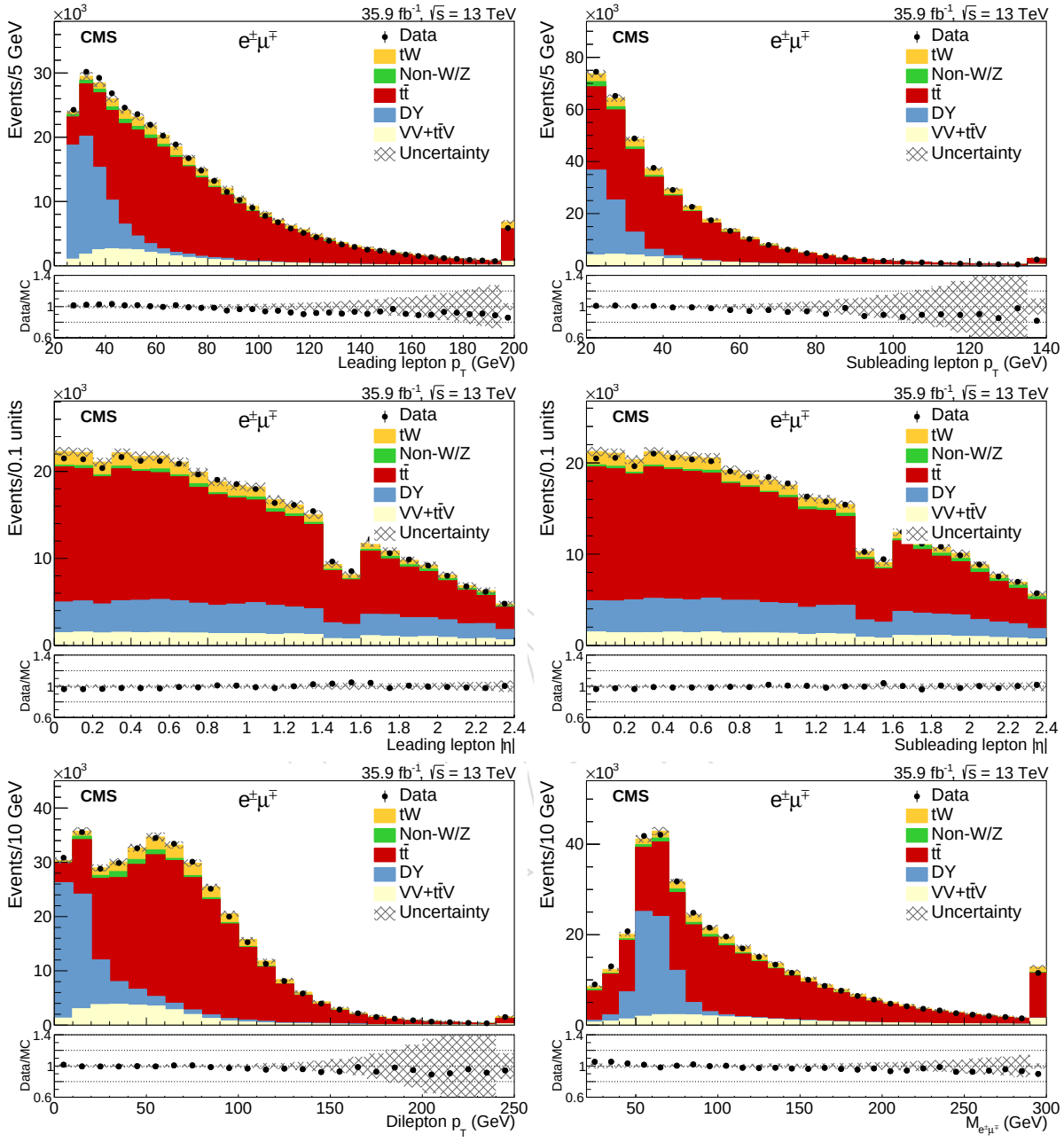

Figure 2: Comparison of the observed data and simulated events for several lepton kinematic variables after the dilepton selection is applied. The error band includes the statistical and systematic uncertainties. The bottom of each panel shows the ratios of data to the sum of the expected yields.

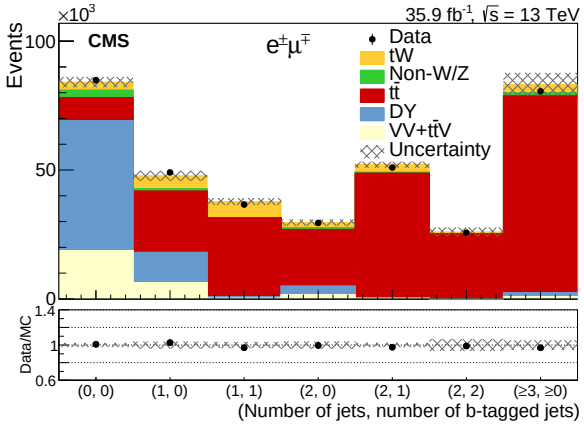

Figure 3: Yields observed in data compared with those expected from simulation as a function of the number of jets and number of b-tagged jets for events passing the baseline dileptonic selection. The error band includes the statistical and systematic uncertainties. The bottom of each panel shows the ratios of data to the sum of the expected yields.

- centrality (ratio between the sum of the transverse momentum and the sum of the total momentum) of the jet and the two leptons,
- vector sum of p_{T} of jet and leptons.
- scalar sum of the p_{T} of leptons, jet, and p_T^{miss} (H_T),
- ratio of p_T^{sys} to H_T for the event,
- invariant mass of the combination of the leptons, jet, and p_T^{miss} (M_{sys}),
- number of b-tagged loose jets,

Events in the 2j1b control region also show a reasonable signal to background ratio. In order to gain additional discrimination power a second BDT is trained with events in this category. The input variables used for the training, listed in order of importance to the BDT training, are the following:

- separation in the $\phi - \eta$ space between the dilepton and dijet system ($\Delta R(\mathrm{e}^{\pm}\mu^{\mp}, \mathrm{j}_1 j_2)$),
- separation in the $\phi - \eta$ space between the dilepton system and the dijet and missing transverse momentum system ($\Delta R(\mathrm{e}^{\pm}\mu^{\mp}, \mathrm{j}_1 j_2 E_T^{sys})$).
- p_{T} of the subleading jet,
- separation in the $\phi - \eta$ space between the leading lepton and the leading jet ($\Delta R(\ell_1, j_1)$),

Finally, 2j2b events, a region highly enriched in $\mathrm{t\bar{t}}$ events, are also used in order to constrain the main source of background. In order to do that, the distribution of the p_{T} of the subleading jet is used. This variable is sensitive to jet energy scale variations and, therefore, helpful to constrain this source of systematic uncertainty.

The distributions of the BDT output in the 1j1b and 2j1b categories, and of the p_{T} of the subleading jet in the 2j2b region for data and simulated events are shown in Fig. 4.

The signal is extracted by performing a maximum likelihood fit to data using several distributions. Fit templates for signal and background processes are taken from MC. The distributions from Fig. 4, after changing the binning of the BDT outputs such that each bin contains the same amount of $\mathrm{t\bar{t}}$ background, are included in the fit. This election of binning ensures that enough background events populate all the bins of the distribution, helping to constrain the system-

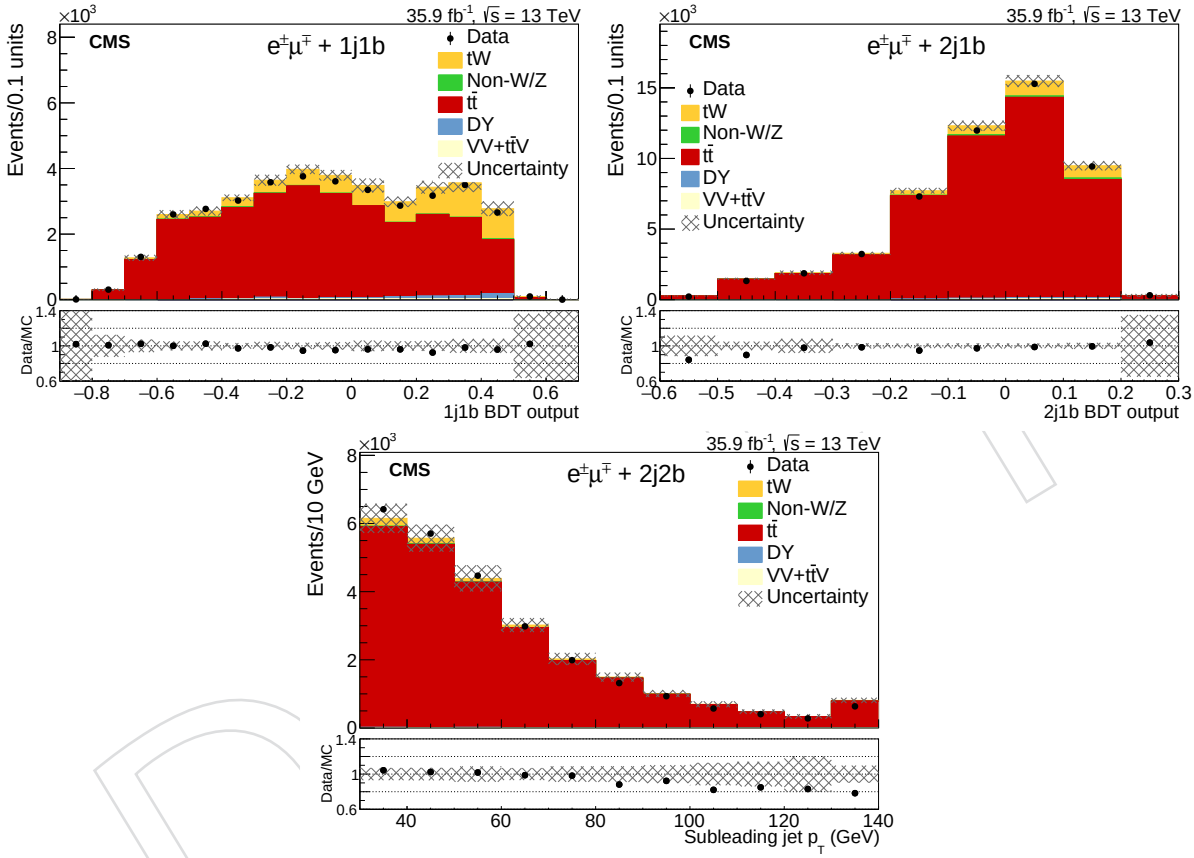

Figure 4: Comparison of the observed data and simulated events for the BDT output in the 1j1b (left) and 2j1b (center) regions and the p_{T} of the subleading jet in the 2j2b region (right). The error band includes the statistical and systematic uncertainties. The bottom of each panel shows the ratios of data to the sum of the expected yields.

atic uncertainties. The fit is performed to extract the tW signal strength parameter, defined as $\mu = \sigma_{tW}/\sigma_{tW}^{SM}$. Comparisons of the final pre-fit distributions of the BDT discriminants in the 1j1b and 2j1b regions as well as the distribution of the subleading jet p_T in the 2j2b region for data and simulated events are shown in Fig. 5.

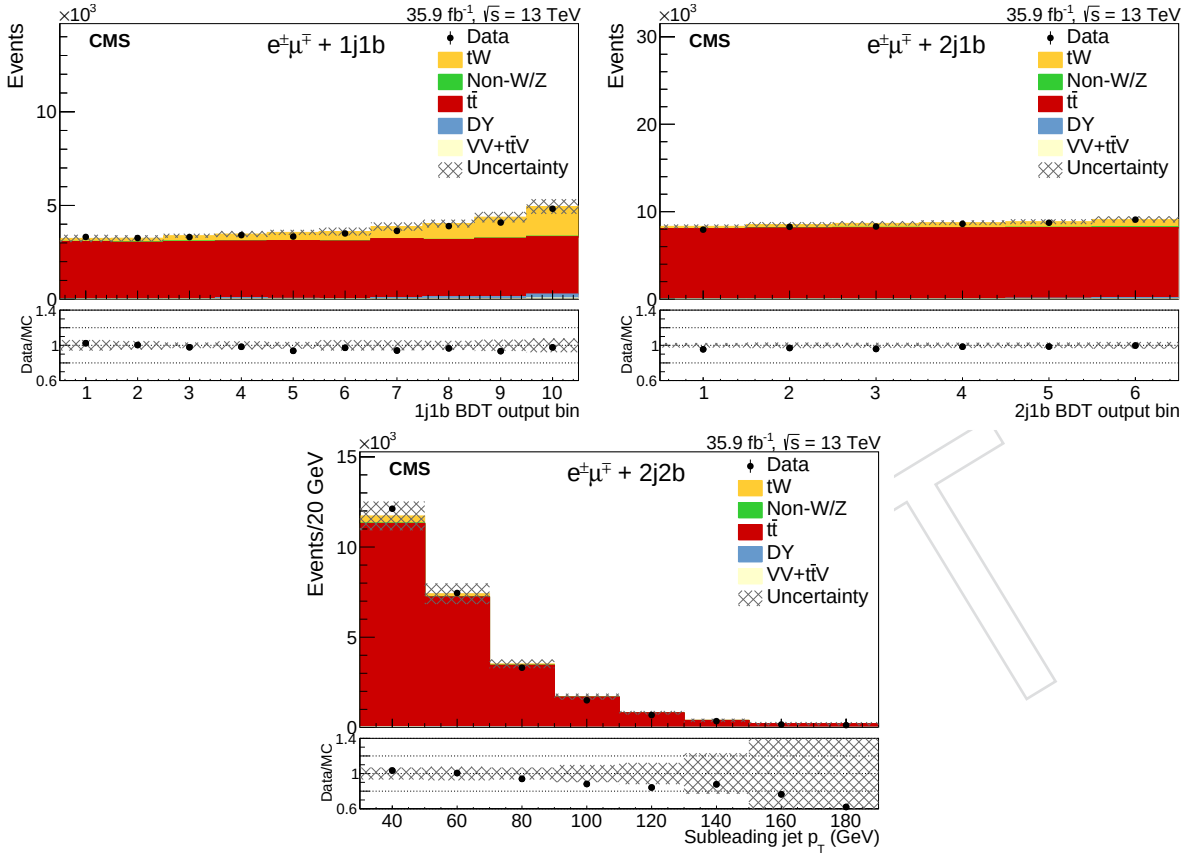

Figure 5: Comparison of the observed data and simulated events for the distributions to which the fit is performed: BDT output in the 1j1b (left) and 2j1b (center) regions and the p_T of the subleading jet in the 2j2b region (right). The binning in the two BDT outputs is chosen such that each bin contains the same amount of $t\bar{t}$ background, while intervals of 20 GeV are taken for the p_T of the subleading jet. The error band includes the statistical and systematic uncertainties. The bottom of each panel shows the ratios of data to the sum of the expected yields.

5 Sources of systematic uncertainty

The measurement of the tW production cross section is affected by different sources of systematic uncertainties that originate from detector effects and from theoretical modeling. Each source of systematic uncertainty is assessed individually by suitable variations of the MC simulations or by variations of parameter values in the analysis within their estimated uncertainties. Each contribution is finally represented by a nuisance parameter which is fit together with the tW production cross section.

5.1 Experimental uncertainties

- The uncertainties on the dilepton trigger and lepton identification efficiencies in simulation are estimated by varying data-to-simulation SFs by their uncertainties.,

which are about 0.7% and 1.5%, respectively, with some dependence on the lepton p_T and η.

- The uncertainty due to the limited knowledge of the jet energy scale and jet energy resolution is determined by varying the scale and resolution within its uncertainties in bins of p_T and η, typically by a few percent [41].
- The uncertainties resulting from the b tagging efficiency and misidentification rate are determined by varying, within their uncertainties, the b tagging data-to-simulation SF of the b jets and the light-flavor jets, respectively. These uncertainties depend on the p_T and η of the jet and amount to approximately 2% for b jets and 10% for mistagged jets [44] as measured in simulated $t\bar{t}$ events.
- For $t\bar{t}V$, VV, DY and non-W/Z background contibutions, a conservative normalization uncertainty of $\pm 50\%$ is assumed.
- The uncertainty assigned to the number of pileup events in simulation is obtained by changing the inelastic proton-proton cross section, which is used to estimate the pileup in data, by $\pm 4.6\%$ [47].
- The uncertainty on the integrated luminosity is estimated to be 2.5% [48].

5.2 Modeling uncertainties

The modeling of the tW signal and $t\bar{t}$ background events by the MC simulation is an important ingredient of the measurement. The impact of theoretical assumptions in the modeling is determined by repeating the analysis and replacing the standard POWHEG +PYTHIA $t\bar{t}$ simulation by dedicated simulation samples with altered parameters.

The uncertainty on modeling of the hard-production process is assessed through changes in the renormalization (μ_R) and factorization (μ_F) scales in the POWHEG sample by factors of two and 0.5 relative to their common nominal value, which is set in POWHEG to $\mu_R = \mu_F = Q = \sqrt{m_t^2 + p_{T,t}^2}$, where $p_{T,t}^2$ denotes the square transverse momentum of the top quark in the $t\bar{t}$ zero-momentum frame.

In order to take into account parton-shower (PS) uncertainties, different effects are studied:

- Underlying event: the parameters of the PYTHIA tune to measurements of the underlying event [21, 24], used to take into account non-pertubative QCD effects, are varied up and down within their uncertainties.
- Matrix element/PS matching: the uncertainty in the combination of the matrix element calculation with the parton shower is estimated from the variation of the POWHEG parameter $h_{damp} = 1.58^{+0.66}_{-0.59} \cdot m_t$, which regulates the damping of real emissions in the NLO calculation when matching to the PS [21].
- Initial (final) state radiation scale: the PS scale used for the simulation of the initial (final) state radiation is varied up and down by a factor of two ($\sqrt{2}$).
- Color reconnection: the effect of multiple-parton interactions and the parameterization of color reconnection have been studied in [24] and are varied accordingly. In addition, we use a simulation with activated color reconnection of resonant decays. The uncertainties that arise from ambiguities in modeling color reconnection effects are estimated by comparing the default model in PYTHIA with two alternative models of color reconnection, a model with string formation beyond leading color [49] and a model in that the gluons can be moved to another string [50]. All models are tuned to measurements of the underlying event [21, 24].

The uncertainty from the choice of PDFs is determined by reweighting the sample of simulated $t\bar{t}$ events according to the 100 NNPDF3.0 error PDF sets [17]. The root-mean-square of the distribution is taken as an uncertainty.

Additionally the difference between the DS and DR schemes is taken as a source of systematic uncertainty on the signal.

6 Results

The tW signal strength parameter that results in the best fit to the data is 0.88 ± 0.02 (stat) $\pm$ 0.08 (syst) $\pm$ 0.03 (lumi), corresponding to a measured cross-section of 63.1 ± 1.8 (stat) $\pm$ 5.7 (syst) $\pm$ 2.1 (lumi) pb, consistent with SM expectations.

Comparisons of the final post-fit distributions of the BDT discriminants in the 1j1b and 2j1b regions as well as the distribution of the subleading jet p_T in the 2j2b region for data and simulated events are shown in Fig. 6.

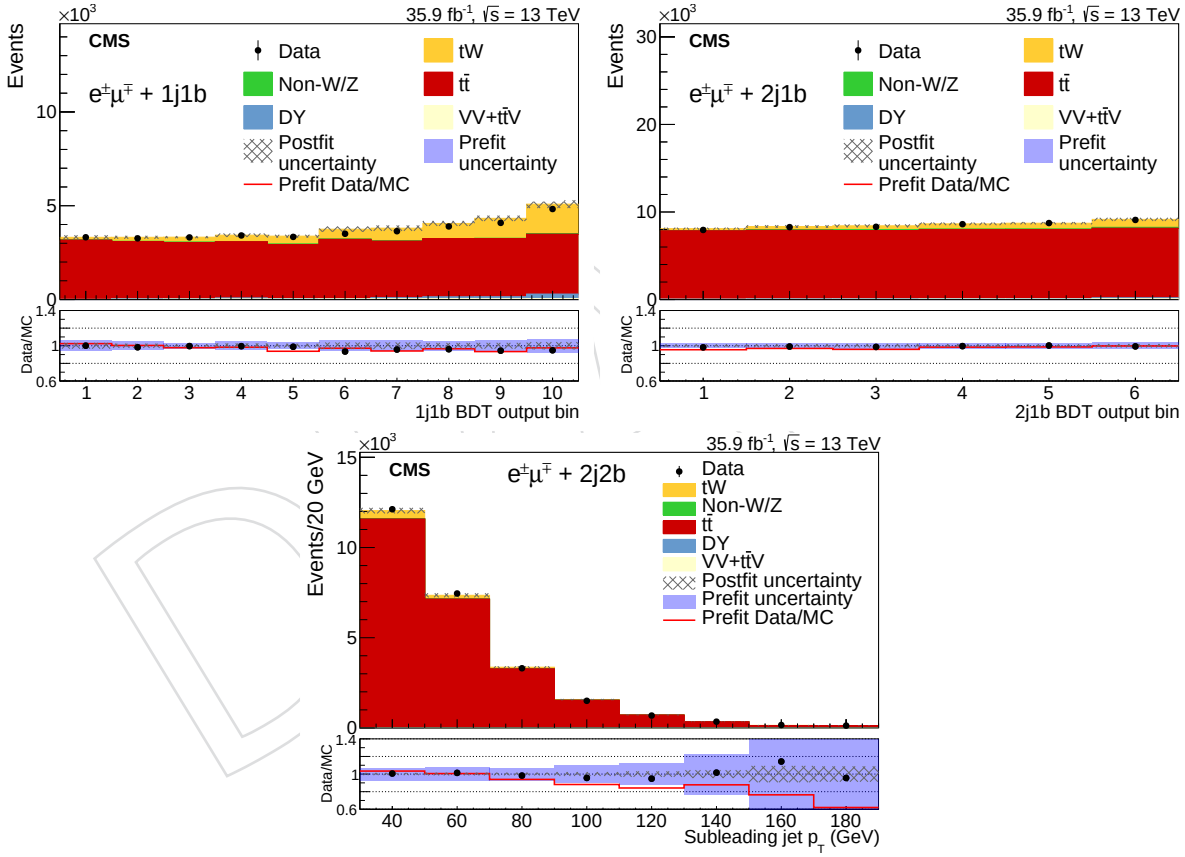

Figure 6: Comparison of the observed data and simulated events for the distributions after the fit is performed: BDT output in the 1j1b (left) and 2j1b (center) regions and the p_T of the subleading jet in the 2j2b region (right). The error band includes the statistical and systematic uncertainties. The bottom of each panel shows the ratios of data to the sum of the expected yields.

The impact of each source of systematic uncertainty in the fit, shown in Table 1, is evaluated by performing the fit fixing the rest of the nuisance parameters to their post-fit value.

Table 1: Estimation of the effect of each source of systematic uncertainty to the fit.

Source	Uncertainty (%)
Trigger efficiencies	2.7
Muon efficiencies	3.1
Electron efficiencies	3.2
Jet energy scale	3.2
Jet energy resolution	1.8
b tagging efficiency	1.4
Mistagging rate	0.2
Pileup	3.3
μ_R and μ_F scale	2.7
Underlying event	0.4
ME/PS matching	1.8
Initial state radiation	0.8
Final state radiation	0.8
Color reconnection	2.0
PDF	1.5
DR-DS	1.3
VV normalization	0.4
Drell–Yan normalization	1.1
Non-W/Z leptons normalization	1.6
$t\bar{t}V$ normalization	0.1
MC statistics	1.6
Total systematic (excluding integrated luminosity)	9.1
Integrated luminosity	3.3
Statistical	2.8
Total	10.1

7 Summary

The full data set recorded by CMS at 13 TeV during 2016, corresponding to an integrated luminosity of 35.9 ± 0.9 fb^{-1}, is used to measure the tW production cross section in the $e^{\pm}\mu^{\mp}$ channel. The signal is measured using a maximum likelihood fit to the distribution of BDT discriminants in the 1j1b and 2j1b categories and the subleading jet p_T distribution in the 2j1b category. The measured cross section of the tW production is found to be $63.1 \pm 1.8\ (\text{stat}) \pm 5.7\ (\text{syst}) \pm 2.1\ (\text{lumi})$ pb. A relative uncertainty of 10% in the tW production cross section is achieved. The measurement, which represents the first one from the CMS experiment at $\sqrt{s}$ = 13 TeV, is consistent with the standard model prediction of $71.7 \pm 1.8\ (\text{scale}) \pm 3.4\ (\text{PDF})$ pb and with a similar measurement by the ATLAS collaboration [13] .

Acknowledgments

We congratulate our colleagues in the CERN accelerator departments for the excellent performance of the LHC and thank the technical and administrative staffs at CERN and at other CMS institutes for their contributions to the success of the CMS effort. In addition, we gratefully acknowledge the computing centres and personnel of the Worldwide LHC Computing Grid for delivering so effectively the computing infrastructure essential to our analyses. Finally, we acknowledge the enduring support for the construction and operation of the LHC

and the CMS detector provided by the following funding agencies: the Austrian Federal Ministry of Science, Research and Economy and the Austrian Science Fund; the Belgian Fonds de la Recherche Scientifique, and Fonds voor Wetenschappelijk Onderzoek; the Brazilian Funding Agencies (CNPq, CAPES, FAPERJ, and FAPESP); the Bulgarian Ministry of Education and Science; CERN; the Chinese Academy of Sciences, Ministry of Science and Technology, and National Natural Science Foundation of China; the Colombian Funding Agency (COLCIENCIAS); the Croatian Ministry of Science, Education and Sport, and the Croatian Science Foundation; the Research Promotion Foundation, Cyprus; the Secretariat for Higher Education, Science, Technology and Innovation, Ecuador; the Ministry of Education and Research, Estonian Research Council via IUT23-4 and IUT23-6 and European Regional Development Fund, Estonia; the Academy of Finland, Finnish Ministry of Education and Culture, and Helsinki Institute of Physics; the Institut National de Physique Nucléaire et de Physique des Particules / CNRS, and Commissariat à l'Énergie Atomique et aux Énergies Alternatives / CEA, France; the Bundesministerium für Bildung und Forschung, Deutsche Forschungsgemeinschaft, and Helmholtz-Gemeinschaft Deutscher Forschungszentren, Germany; the General Secretariat for Research and Technology, Greece; the National Scientific Research Foundation, and National Innovation Office, Hungary; the Department of Atomic Energy and the Department of Science and Technology, India; the Institute for Studies in Theoretical Physics and Mathematics, Iran; the Science Foundation, Ireland; the Istituto Nazionale di Fisica Nucleare, Italy; the Ministry of Science, ICT and Future Planning, and National Research Foundation (NRF), Republic of Korea; the Lithuanian Academy of Sciences; the Ministry of Education, and University of Malaya (Malaysia); the Mexican Funding Agencies (BUAP, CINVESTAV, CONACYT, LNS, SEP, and UASLP-FAI); the Ministry of Business, Innovation and Employment, New Zealand; the Pakistan Atomic Energy Commission; the Ministry of Science and Higher Education and the National Science Centre, Poland; the Fundação para a Ciência e a Tecnologia, Portugal; JINR, Dubna; the Ministry of Education and Science of the Russian Federation, the Federal Agency of Atomic Energy of the Russian Federation, Russian Academy of Sciences, the Russian Foundation for Basic Research and the Russian Competitiveness Program of NRNU "MEPhI"; the Ministry of Education, Science and Technological Development of Serbia; the Secretaría de Estado de Investigación, Desarrollo e Innovación, Programa Consolider-Ingenio 2010, Plan de Ciencia, Tecnología e Innovación 2013-2017 del Principado de Asturias and Fondo Europeo de Desarrollo Regional, Spain; the Swiss Funding Agencies (ETH Board, ETH Zurich, PSI, SNF, UniZH, Canton Zurich, and SER); the Ministry of Science and Technology, Taipei; the Thailand Center of Excellence in Physics, the Institute for the Promotion of Teaching Science and Technology of Thailand, Special Task Force for Activating Research and the National Science and Technology Development Agency of Thailand; the Scientific and Technical Research Council of Turkey, and Turkish Atomic Energy Authority; the National Academy of Sciences of Ukraine, and State Fund for Fundamental Researches, Ukraine; the Science and Technology Facilities Council, UK; the US Department of Energy, and the US National Science Foundation.

Individuals have received support from the Marie-Curie programme and the European Research Council and Horizon 2020 Grant, contract No. 675440 (European Union); the Leventis Foundation; the A. P. Sloan Foundation; the Alexander von Humboldt Foundation; the Belgian Federal Science Policy Office; the Fonds pour la Formation à la Recherche dans l'Industrie et dans l'Agriculture (FRIA-Belgium); the Agentschap voor Innovatie door Wetenschap en Technologie (IWT-Belgium); the Ministry of Education, Youth and Sports (MEYS) of the Czech Republic; the Council of Scientific and Industrial Research, India; the HOMING PLUS programme of the Foundation for Polish Science, cofinanced from European Union, Regional Development Fund, the Mobility Plus programme of the Ministry of Science and Higher Education, the National Science Center (Poland), contracts Harmonia 2014/14/M/ST2/00428,

Opus 2014/13/B/ST2/02543, 2014/15/B/ST2/03998, and 2015/19/B/ST2/02861, Sonata-bis 2012/07/E/ST2/01406; the National Priorities Research Program by Qatar National Research Fund; the Programa Clarín-COFUND del Principado de Asturias; the Thalis and Aristeia programmes cofinanced by EU-ESF and the Greek NSRF; the Rachadapisek Sompot Fund for Postdoctoral Fellowship, Chulalongkorn University and the Chulalongkorn Academic into Its 2nd Century Project Advancement Project (Thailand); and the Welch Foundation, contract C-1845.

References

[1] CDF Collaboration, "First Observation of Electroweak Single Top Quark Production", *Phys. Rev. Lett.* **103** (2009) 092002, doi:10.1103/PhysRevLett.103.092002, arXiv:0903.0885.

[2] D0 Collaboration, "Observation of Single Top Quark Production", *Phys. Rev. Lett.* **103** (2009) 092001, doi:10.1103/PhysRevLett.103.092001, arXiv:0903.0850.

[3] S. Frixione et al., "Single-top hadroproduction in association with a W boson", *JHEP* **07** (2008) 029, doi:10.1088/1126-6708/2008/07/029, arXiv:0805.3067.

[4] A. S. Belyaev, E. E. Boos, and L. V. Dudko, "Single top quark at future hadron colliders: Complete signal and background study", *Phys. Rev. D* **59** (1999) 075001, doi:10.1103/PhysRevD.59.075001, arXiv:hep-ph/9806332.

[5] C. D. White, S. Frixione, E. Laenen, and F. Maltoni, "Isolating Wt production at the LHC", *JHEP* **11** (2009) 074, doi:10.1088/1126-6708/2009/11/074, arXiv:0908.0631.

[6] T. M. P. Tait and C. P. Yuan, "Single top quark production as a window to physics beyond the standard model", *Phys. Rev. D* **63** (2000) 014018, doi:10.1103/PhysRevD.63.014018, arXiv:hep-ph/0007298.

[7] Q.-H. Cao, J. Wudka, and C. P. Yuan, "Search for new physics via single top production at the LHC", *Phys. Lett. B* **658** (2007) 50–56, doi:10.1016/j.physletb.2007.10.057, arXiv:0704.2809.

[8] V. Barger, M. McCaskey, and G. Shaughnessy, "Single top and Higgs associated production at the LHC", *Phys. Rev. D* **81** (2010) 034020, doi:10.1103/PhysRevD.81.034020, arXiv:0911.1556.

[9] CMS Collaboration, "Evidence for associated production of a single top quark and W boson in pp collisions at $\sqrt{s}$ = 7 TeV", *Phys. Rev. Lett.* **110** (2013) 022003, doi:10.1103/PhysRevLett.110.022003, arXiv:1209.3489.

[10] ATLAS Collaboration, "Evidence for the associated production of a W boson and a top quark in ATLAS at $\sqrt{s} = 7$ TeV", *Phys. Lett. B* **716** (2012) 142–159, doi:10.1016/j.physletb.2012.08.011, arXiv:1205.5764.

[11] CMS Collaboration, "Observation of the associated production of a single top quark and a W boson in pp collisions at $\sqrt{s}$ =8 TeV", *Phys. Rev. Lett.* **112** (2014), no. 23, 231802, doi:10.1103/PhysRevLett.112.231802, arXiv:1401.2942.

[12] ATLAS Collaboration, "Measurement of the production cross-section of a single top quark in association with a W boson at 8 TeV with the ATLAS experiment", *JHEP* **01** (2016) 064, doi:10.1007/JHEP01(2016)064, arXiv:1510.03752.

[13] ATLAS Collaboration, "Measurement of the cross-section for producing a W boson in association with a single top quark in pp collisions at $\sqrt{s} = 13$TeV with ATLAS", arXiv:1612.07231.

[14] N. Kidonakis, "Theoretical results for electroweak-boson and single-top production", *PoS* **DIS2015** (2015) 170, arXiv:1506.04072.

[15] CMS Collaboration, "The CMS experiment at the CERN LHC", *JINST* **3** (2008) S08004, doi:10.1088/1748-0221/3/08/S08004.

[16] E. Re, "Single-top Wt-channel production matched with parton showers using the POWHEG method", *Eur. Phys. J. C* **71** (2011) 1547, doi:10.1140/epjc/s10052-011-1547-z, arXiv:1009.2450.

[17] NNPDF Collaboration, "Parton distributions for the LHC Run II", *JHEP* **04** (2015) 040, doi:10.1007/JHEP04(2015)040, arXiv:1410.8849.

[18] T. Sjöstrand, S. Mrenna, and P. Skands, "PYTHIA 6.4 physics and manual", *JHEP* **05** (2006) 026, doi:10.1088/1126-6708/2006/05/026, arXiv:hep-ph/0603175.

[19] T. Sjostrand et al., "An Introduction to PYTHIA 8.2", *Comput. Phys. Commun.* **191** (2015) 159, doi:10.1016/j.cpc.2015.01.024, arXiv:1410.3012.

[20] CMS Collaboration, "Underlying Event Tunes and Double Parton Scattering", Technical Report CMS-PAS-GEN-14-001, CERN, Geneva, 2014.

[21] P. Skands, S. Carrazza, and J. Rojo, "Tuning PYTHIA 8.1: the Monash 2013 Tune", *Eur. Phys. J. C* **74** (2014), no. 8, 3024, doi:10.1140/epjc/s10052-014-3024-y, arXiv:1404.5630.

[22] T. M. P. Tait, "tW^- mode of single top quark production", *Phys. Rev. D* **61** (1999) 034001, doi:10.1103/PhysRevD.61.034001.

[23] S. Alioli et al., "A general framework for implementing NLO calculations in shower Monte Carlo programs: the POWHEG BOX", *JHEP* **06** (2010) 043, doi:10.1007/JHEP06(2010)043, arXiv:1002.2581.

[24] CMS Collaboration, "Investigations of the impact of the parton shower tuning in Pythia 8 in the modelling of $\mathrm{t\bar{t}}$ at $\sqrt{s} = 8$ and 13 TeV", Technical Report CMS-PAS-TOP-16-021, CERN, Geneva, 2016.

[25] J. Alwall et al., "The automated computation of tree-level and next-to-leading order differential cross sections, and their matching to parton shower simulations", *JHEP* **07** (2014) 079, doi:10.1007/JHEP07(2014)079, arXiv:1405.0301.

[26] R. Frederix and S. Frixione, "Merging meets matching in MC@NLO", *JHEP* **12** (2012) 061, doi:10.1007/JHEP12(2012)061, arXiv:1209.6215.

[27] Y. Li and F. Petriello, "Combining QCD and electroweak corrections to dilepton production in the framework of the FEWZ simulation code", *Phys. Rev. D* **86** (2012) 094034, doi:10.1103/PhysRevD.86.094034.

[28] J. M. Campbell, R. K. Ellis, and C. Williams, "Vector boson pair production at the LHC", *JHEP* **07** (2011) 018, doi:10.1007/JHEP07(2011)018, arXiv:1105.0020.

[29] M. Czakon and A. Mitov, "Top++: A Program for the Calculation of the Top-Pair Cross-Section at Hadron Colliders", *Comput. Phys. Commun.* **185** (2014) 2930, doi:10.1016/j.cpc.2014.06.021, arXiv:1112.5675.

[30] S. Alekhin et al., "The PDF4LHC Working Group Interim Report", arXiv:1101.0536.

[31] M. Botje et al., "The PDF4LHC Working Group Interim Recommendations", arXiv:1101.0538.

[32] H.-L. Lai et al., "New parton distributions for collider physics", *Phys. Rev. D* **82** (2010) 074024, doi:10.1103/PhysRevD.82.074024, arXiv:1007.2241.

[33] J. Gao et al., "CT10 next-to-next-to-leading order global analysis of QCD", *Phys. Rev. D* **89** (2014) 033009, doi:10.1103/PhysRevD.89.033009, arXiv:1302.6246.

[34] NNPDF Collaboration, "Parton distributions with LHC data", *Nucl. Phys. B* **867** (2013) 244, doi:10.1016/j.nuclphysb.2012.10.003, arXiv:1207.1303.

[35] CMS Collaboration, "Measurement of the $t\bar{t}$ production cross section using events in the eμ final state in pp collisions at $\sqrt{s} = 13$ TeV", *Eur. Phys. J. C* **77** (2017) 172, doi:10.1140/epjc/s10052-017-4718-8, arXiv:1611.04040.

[36] CMS Collaboration, "Particle-flow reconstruction and global event description with the CMS detector", arXiv:1706.04965. Submitted to *JINST*.

[37] CMS Collaboration, "Performance of electron reconstruction and selection with the CMS detector in proton-proton collisions at $\sqrt{s} = 8$ TeV", *JINST* **10** (2015) P06005, doi:10.1088/1748-0221/10/06/P06005.

[38] CMS Collaboration, "Performance of CMS muon reconstruction in pp collision events at $\sqrt{s} = 7$ TeV", *JINST* **7** (2012) P10002, doi:10.1088/1748-0221/7/10/P10002, arXiv:1206.4071.

[39] M. Cacciari, G. P. Salam, and G. Soyez, "The anti-k_t jet clustering algorithm", *JHEP* **04** (2008) 063, doi:10.1088/1126-6708/2008/04/063, arXiv:0802.1189.

[40] M. Cacciari, G. P. Salam, and G. Soyez, "FastJet user manual", *Eur. Phys. J. C* **72** (2012) 1896, doi:10.1140/epjc/s10052-012-1896-2, arXiv:1111.6097.

[41] CMS Collaboration Collaboration, "Jet algorithms performance in 13 TeV data", Technical Report CMS-PAS-JME-16-003, CERN, Geneva, 2017.

[42] CMS Collaboration, "Performance of missing energy reconstruction in $\sqrt{s} = 13$ TeV pp collision data using the CMS detector", Technical Report CMS-PAS-JME-16-004, CERN, Geneva, 2016.

[43] CMS Collaboration, "Identification of b-quark jets with the CMS experiment", *JINST* **8** (2013) P04013, doi:10.1088/1748-0221/8/04/P04013, arXiv:1211.4462.

[44] CMS Collaboration, "Identification of b quark jets at the CMS experiment in the LHC Run2", CMS Physics Analysis Summary CMS-PAS-BTV-15-001, 2016.

[45] J. H. Friedman, "Stochastic gradient boosting", *Computational Statistics & Data Analysis* **38** (2002), no. 4, 367, doi:https://doi.org/10.1016/S0167-9473(01)00065-2. Nonlinear Methods and Data Mining.

[46] H. Voss, A. Höcker, J. Stelzer, and F. Tegenfeldt, "TMVA, the Toolkit for Multivariate Data Analysis with ROOT", in *XI International Workshop on Advanced Computing and Analysis Techniques in Physics Research*, p. 040. SISSA, 2007. arXiv:physics/0703039. PoS(ACAT2007)040.

[47] ATLAS Collaboration, "Measurement of the Inelastic Proton-Proton Cross Section at $\sqrt{s} = 13$ TeV with the ATLAS Detector at the LHC", *Phys. Rev. Lett.* **117** (2016) 182002, doi:10.1103/PhysRevLett.117.182002, arXiv:1606.02625.

[48] CMS Collaboration, "CMS Luminosity Measurements at 13 TeV - Winter 2017 update", CMS Physics Analysis Summary CMS-PAS-LUMI-17-001, 2017.

[49] J. R. Christiansen and P. Z. Skands, "String Formation Beyond Leading Colour", *JHEP* **08** (2015) 003, doi:10.1007/JHEP08(2015)003, arXiv:1505.01681.

[50] S. Argyropoulos and T. Sjstrand, "Effects of color reconnection on $t\bar{t}$ final states at the LHC", *JHEP* **11** (2014) 043, doi:10.1007/JHEP11(2014)043, arXiv:1407.6653.

A Supplemental Material

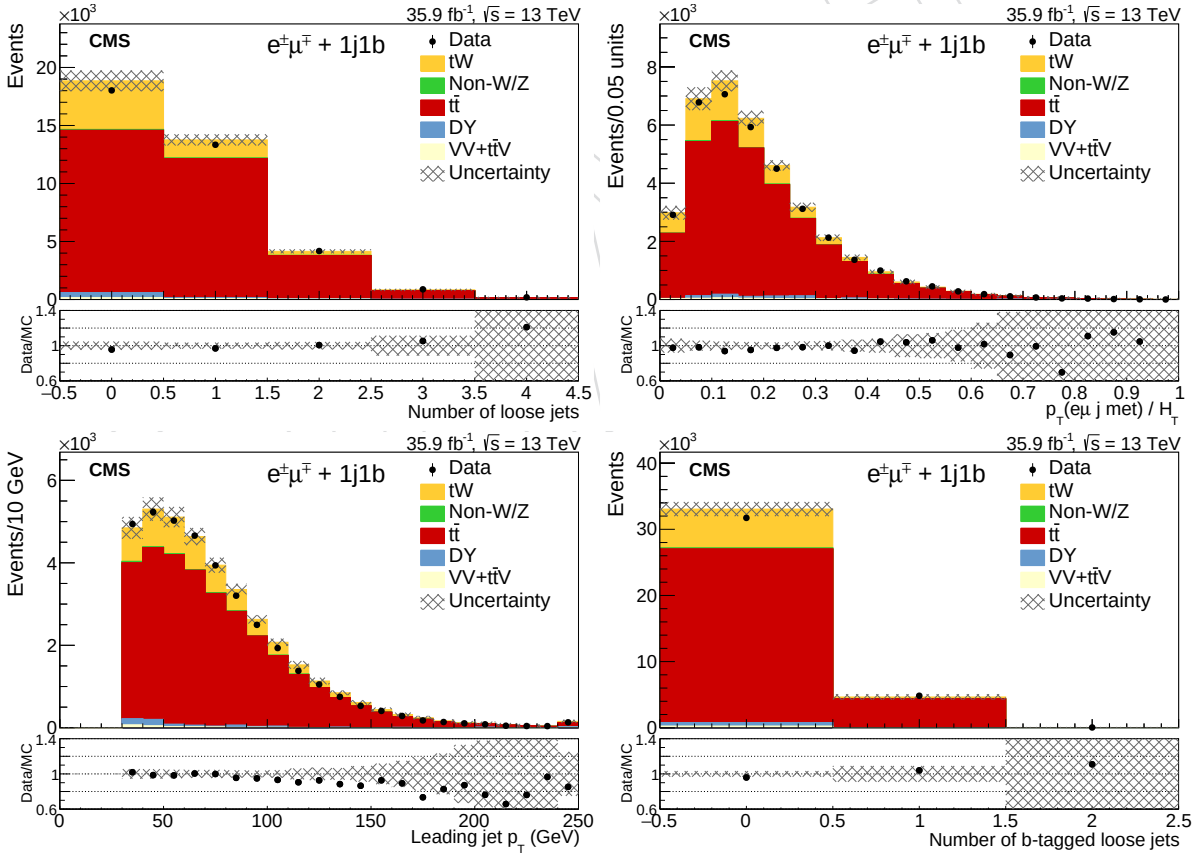

Figure 7: Variables used for the training of the BDT in the 1j1b category. The error band includes the statistical and systematic uncertainties. The bottom of each panel shows the ratios of data to the sum of the expected yields.

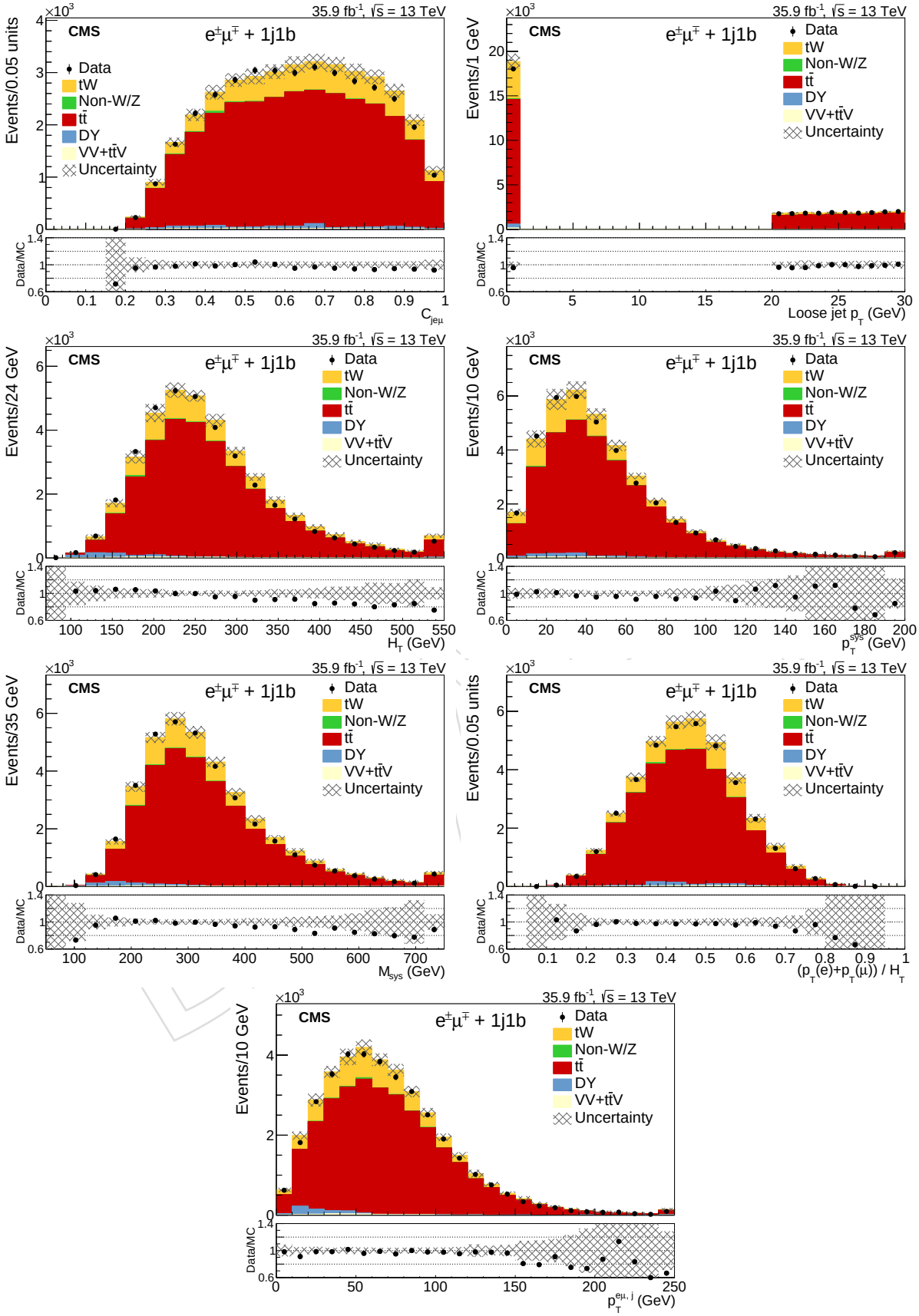

Figure 8: Variables used for the training of the BDT in the 1j1b category. The error band includes the statistical and systematic uncertainties. The bottom of each panel shows the ratios of data to the sum of the expected yields.

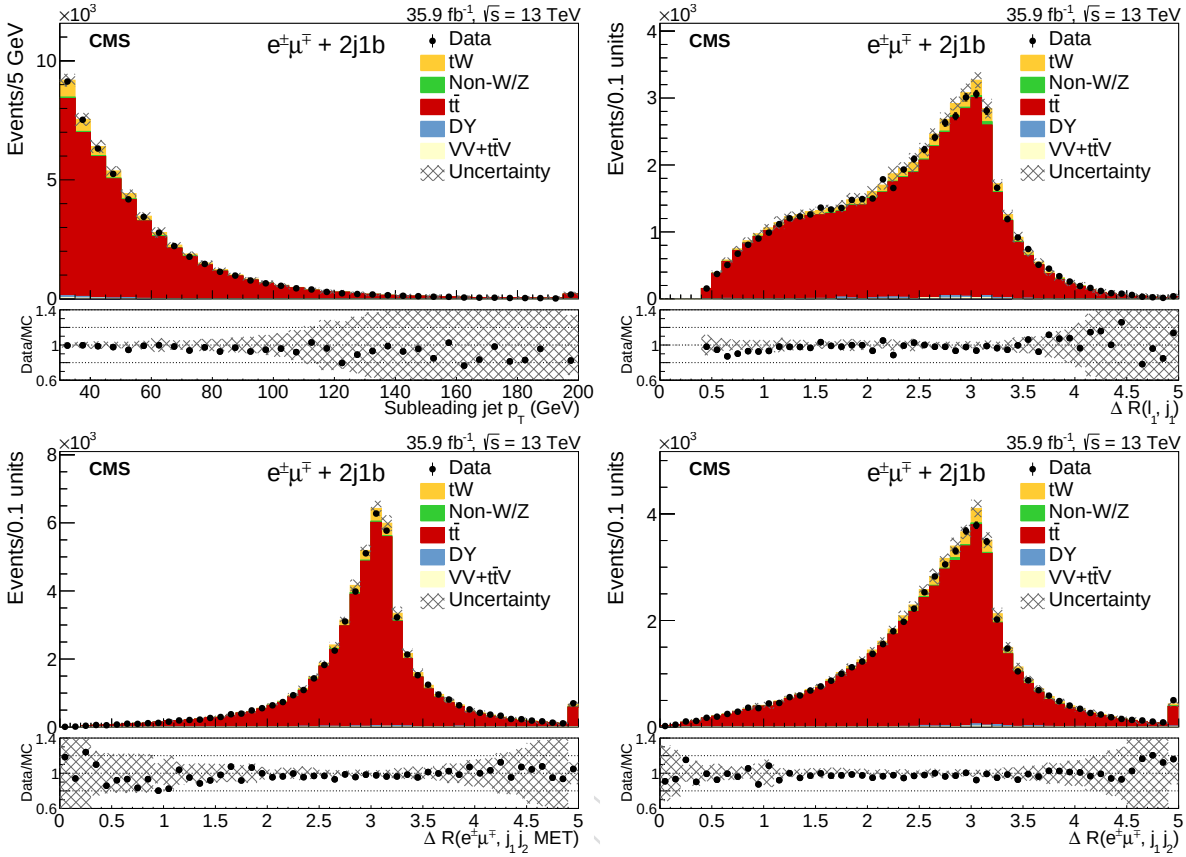

Figure 9: Variables used for the training of the BDT in the 2j1b category. The error band includes the statistical and systematic uncertainties. The bottom of each panel shows the ratios of data to the sum of the expected yields.

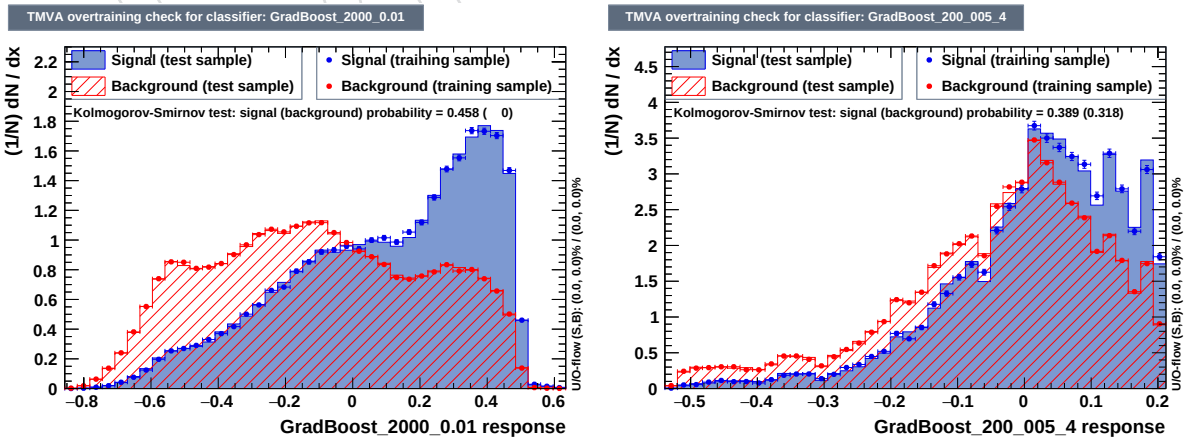

Figure 10: Comparison of the BDT output in the 1j1b (left) and 2j1b (right) category. The distributions for signal and backgorund events in the training and tests sampes are shown.